Adaptive Compensation Scheme for Wireless Power Transfer Systems with Coil Inductance Variation Using PWM-Controlled Switched Capacitor

Ryo Matsumoto[1], Hiroshi Fujimoto[2]
[1,2]Graduate School of Frontier Sciences, The University of Tokyo, Kashiwa, Japan
[1]matsumoto.ryo19@ae.k.u-tokyo.ac.jp, [2]fujimoto@k.u-tokyo.ac.jp

***Abstract*—Wireless power transfer (WPT) via magnetic resonance coupling is characterized by the use of compensation capacitors to tune the resonant frequency of the system. However, the system becomes mistuned when the self-inductance of the transmitter (Tx) and receiver (Rx) coils vary due to misalignment or manufacturing tolerance of the coils. This paper proposes a control scheme of pulsewidth modulation controlled switched capacitors to compensate for the self-inductance variations in WPT systems. The control scheme proposed in this paper does not require wireless communication between the primary and secondary sides or any additional components besides the switched capacitors. The principle of the control scheme is explained based on a steady-state analysis of the WPT circuit, and its validity is verified through experimental results of a 40-W prototype.**

***Keywords*—Wireless power transfer, switched capacitor, resonant frequency, self-inductance variation, mistuning.**

I. Introduction

Wireless power transfer (WPT) is gaining attention as a convenient way to charge various electronic devices such as biomedical implants, mobile phones, Internet of Things, and electric vehicles (EVs) [1]–[4]. In particular, WPT via magnetic resonance coupling is increasingly gaining attention from various fields in the industry [5]–[7]. This technique improves the power transfer characteristics by tuning the resonant frequencies of the primary and secondary circuits with compensation capacitors. However, the system becomes mistuned when the self-inductance of the transmitter (Tx) and receiver (Rx) coils vary from their designed values for the following reasons. The Tx and Rx coils are usually equipped with magnetic and conductive materials, which make the self-inductance of the coils sensitive to misalignment [8], [9]. In addition, the manufacturing tolerance of the coils and other magnetic and conductive materials in the environment cause the self-inductance of the coils to vary even more [10], [11].

Several methods have been proposed to compensate for the self-inductance variations in the literature [12]–[16]. Kim and Ahn [12] proposed a self-tuning LCC inverter using a pulsewidth modulation (PWM) controlled switched capacitor. However, this study focused only on the self-inductance variation of the Tx coil. Ahn *et al.* [13] proposed an impedance tuning control for semi-bridgeless active rectifiers to compensate for the impedance mismatch in wireless EV charging. Ishihara *et al.* [14] proposed a control scheme for active reactance compensators to stabilize the output power in multiple-receiver systems. While these studies covered the self-inductance variations of both the Tx and Rx coils, the control schemes required wireless communication between the primary and secondary sides. Mai *et al.* [15] proposed a control method to track the maximum efficiency using an active single-phase rectifier. However, the control scheme required an auxiliary measurement coil in order to avoid wireless communication between the primary and secondary sides.

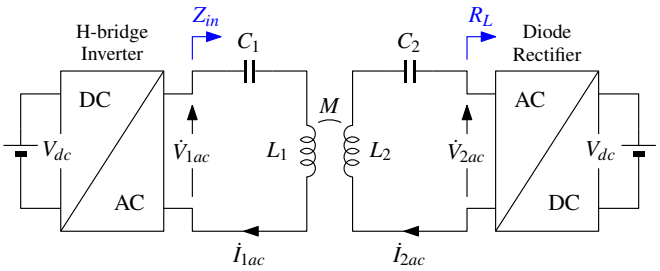

Fig. 1: Simplified circuit model of the SS compensated WPT system.

The studies in [12]–[14] were based on the circuit model of the WPT system with a resistive load. However, the purpose of most WPT systems is to provide power to a battery, which is a constant voltage load. Therefore, this paper proposes a control scheme of PWM-controlled switched capacitors to compensate for the self-inductance variations in WPT systems with a constant voltage load. The proposed control scheme does not require wireless communication between the primary and secondary sides or any additional components besides the switched capacitors, thus enabling its use in a wide range of applications.

II. Circuit Analysis of Inductance Variation

Fig. 1 shows a simplified circuit model of a series-series (SS) compensated WPT system. L_1 and L_2 represent the self-inductance of the Tx and Rx coils. C_1 and C_2 represent the compensation capacitance of the primary and secondary sides. The primary and secondary dc link voltages are assumed to be symmetrical, and the equivalent series resistance of the primary and secondary circuits are neglected in order to simplify the analysis. In addition, it is assumed that the

inverter is operating at full duty cycle, and a conventional diode-rectifier is adopted on the secondary side. Based on these assumptions, the root mean square values of $\dot{V}_{1ac}$ and $\dot{V}_{2ac}$ can be expressed as:

$$\left|\dot{V}_{1ac}\right| = \left|\dot{V}_{2ac}\right| = \frac{2\sqrt{2}}{\pi} V_{dc}. \tag{1}$$

By applying Kirchhoff's voltage law to the circuit model in Fig. 1, the following equations can be derived:

$$\dot{V}_{1ac} = \left(j\omega L_1 + \frac{1}{j\omega C_1}\right)\dot{I}_{1ac} - j\omega M \dot{I}_{2ac}, \tag{2}$$

$$0 = j\omega M \dot{I}_{1ac} - \left(j\omega L_2 + \frac{1}{j\omega C_2} + R_L\right)\dot{I}_{2ac}. \tag{3}$$

R_L represents the input impedance of the diode rectifier. The equivalent reactance of L_1 and C_1 in series is defined as X_1, and the equivalent reactance of L_2 and C_2 in series is defined as X_2 as:

$$X_1 := \omega L_1 - \frac{1}{\omega C_1}, \quad X_2 := \omega L_2 - \frac{1}{\omega C_2}. \tag{4}$$

When the circuit is perfectly tuned, X_1 and X_2 are equal to zero. When the circuit is mistuned due to the self-inductance variations of the coils, X_1 and X_2 are not equal to zero. Under constant voltage load conditions, R_L is not a constant, since R_L varies depending on the coupling condition and tuning condition of the circuit. By solving (1)–(4), R_L can be expressed in terms of X_1, X_2 and M as:

$$R_L = \left|(\omega M)^2 - X_1 X_2\right| \Big/ \sqrt{(\omega M)^2 - X_1^2}\,. \tag{5}$$

Therefore, the transmission power P can be expressed in terms of X_1, X_2 and the constants defined in Fig. 1 as:

$$P = \frac{4V_{dc}^2}{\pi^2}\sqrt{(\omega M)^2 - X_1^2} \Big/ \left|(\omega M)^2 - X_1 X_2\right|. \tag{6}$$

From Fig. 1, the impedance at the input of the circuit Z_{in} can be derived as:

$$Z_{in} = \frac{R_L(\omega M)^2}{R_L^2 + X_2^2} + j\left[X_1 - \frac{X_2(\omega M)^2}{R_L^2 + X_2^2}\right]. \tag{7}$$

Therefore, the phase difference θ between $\dot{V}_{1ac}$ and $\dot{I}_{1ac}$ can be derived as:

$$\begin{aligned}\theta &= \arctan\left(\frac{\mathrm{Im[Z_{in}]}}{\mathrm{Re[Z_{in}]}}\right) \\ &= \arctan\left(\frac{X_1(R_L^2 + X_2^2) - X_2(\omega M)^2}{R_L(\omega M)^2}\right)\end{aligned} \tag{8}$$

By substituting (5) into (8) and solving $\theta = 0$, the following solution is derived:

$$X_1 = X_2. \tag{9}$$

By substituting (9) into (6), P can be expressed as a convex downward function:

$$P = \frac{4V_{dc}^2}{\pi^2\sqrt{(\omega M)^2 - X_1^2}} = \frac{4V_{dc}^2}{\pi^2\sqrt{(\omega M)^2 - X_2^2}} \tag{10}$$

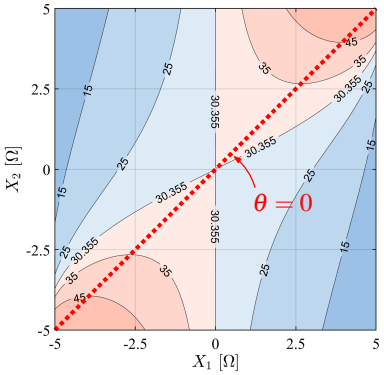

Fig. 2: Colormap of P_2 as a function of X_1 and X_2. V_{dc}, M and ω are 20 V, 10 µH and $2\pi \times 85$ rad s^{-1}, respectively.

Equation (10) indicates that the minimum point of P under $\theta = 0$ is given by:

$$X_1 = X_2 = 0 \tag{11}$$

In other words, the circuit is perfectly tuned when the transmission power is minimized under the condition of $\theta = 0$.

The same conclusion can be drawn by a graphical explanation. Fig. 2 shows the colormap of P as a function of X_1 and X_2, obtained from (6). The colormap is obtained assuming that V_{dc}, M and ω are 20 V, 10 µH and $2\pi \times 85$ rad s^{-1}, respectively. The set of points which satisfy $\theta = 0$ is shown in the red dotted line in Fig. 2. The origin of the colormap *i.e.* $X_1 = X_2 = 0$ coincides with the minimum point on the red dotted line. In fact, the circuit is perfectly tuned when the transmission power is minimized under $\theta = 0$.

III. Control Scheme of PWM-Controlled Switched Capacitor

Fig. 3 shows the circuit configuration and the control scheme of the system proposed to compensate X_1 and X_2. The primary full-bridge inverter supplies high-frequency current to the Tx coil, while the secondary full-bridge inverter conducts synchronous rectification. PWM-controlled switched capacitors proposed in [17] are adopted on the primary and secondary sides to compensate X_1 and X_2. The equivalent capacitance of the switched capacitor is adjusted by feeding a PWM signal synchronized with the current to the MOSFET. The equivalent capacitance C_{1eq} and C_{2eq} can be expressed in terms of the PWM duty cycles d_1 and d_2 as:

$$C_{1eq} = \frac{1}{\frac{1}{C_{11}} + \frac{1}{C_{12}}\left[1 + \frac{1}{2\pi}\sin(2\pi d_1) - d_1\right]}, \tag{12}$$

$$C_{2eq} = \frac{1}{\frac{1}{C_{21}} + \frac{1}{C_{22}}\left[1 + \frac{1}{2\pi}\sin(2\pi d_2) - d_2\right]}. \tag{13}$$

The circuit topology of the PWM-controlled switched capacitor used in this paper is applicable to a wide range of power scales, since this toplogy can suppress the voltage stress on the MOSFET [17].

The most straightforward way to compensate X_1 and X_2 is to directly control the phase difference between v_{1ac} and

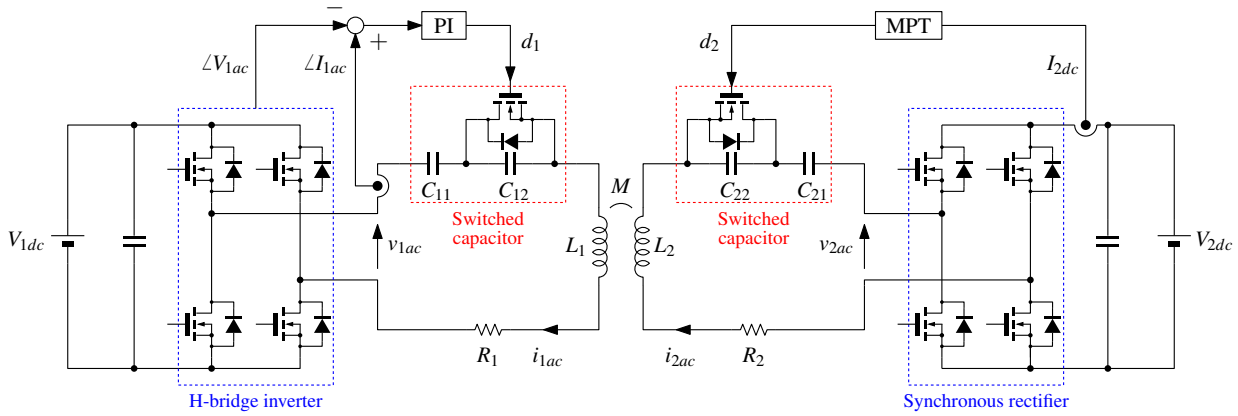

Fig. 3: Circuit configuration and control scheme of the proposed system.

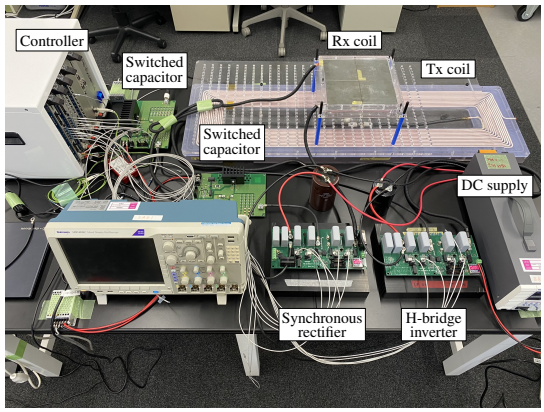

Fig. 4: Experimental setup.

TABLE I: SPECIFICATIONS OF EXPERIMENTAL SETUP.

Symbol	Description	Value
-	Operating frequency	85.0 kHz
V_{1dc}	Primary dc voltage	20.0 V
V_{2dc}	Secondary dc voltage	20.0 V
L_1	Self-inductance of Tx coil	237.5 µH
L_2	Self-inductance of Rx coil	98.6 µH
M	Mutual inductance	15.86 µH
R_1	Equivalent series resistance of Tx coil	245 mΩ
R_2	Equivalent series resistance of Rx coil	152 mΩ
C_{11}	Components of primary switched capacitor	15.76 nF
C_{12}		129.6 nF
C_{21}	Components of secondary switched capacitor	40.43 nF
C_{22}		166.7 nF

i_{1ac} to 0 deg. and the phase difference between i_{1ac} and i_{2ac} to 90 deg. by adjusting the PWM duty cycles of the switched capacitors [13], [14]. However, this solution is unfavorable in terms of reliability and simplicity since wireless communication between the primary and secondary sides is required to obtain the phase difference between i_{1ac} and i_{2ac}. Therefore, the following control scheme for the switched capacitors is adopted. From the analysis in Section II, X_1 and X_2 are perfectly compensated when the output power is minimized under the condition of $\theta = 0$. This can be achieved by controlling the phase difference between v_{1ac} and i_{1ac} to 0 deg. by adjusting the primary switched capacitor, while iteratively searching the minimum output power by adjusting the secondary switched capacitor.

This control scheme can be explained visually based on Fig. 2. By controlling the phase difference between v_{1ac} and i_{1ac} to 0 deg., the coordinate of X_1 and X_2 is constrained to the red dotted line. Then the perfectly tuned state is achieved by searching the minimum power point on the red dotted line.

As shown in Fig. 3, a proportional-integral (PI) controller is adopted to adjust the primary switched capacitor, and a minimum power tracking (MPT) algorithm is implemented to adjust the secondary switched capacitor. Since the secondary dc-link voltage V_{2dc} is constant, the output power is proportional to the secondary dc-link current I_{2dc}. Therefore, a simple hill-climbing algorithm is implemented to search the PWM duty cycle d_2 which yields the minimum I_{2dc}. In order to avoid conflict between the PI controller and the hill-climbing algorithm, the settling time of the PI controller is designed sufficiently faster than the iteration period of the hill-climbing algorithm.

IV. EXPERIMENTAL VERIFICATION

An experimental prototype of the system shown in Fig. 3 is manufactured to verify the proposed control scheme, as shown in Fig. 4. The parameters of the prototype system are listed in Table. I.

Fig. 5 shows the results of a preliminary experiment in which the phase difference between i_{1ac} and i_{2ac} and the input/output power are measured as a function of the PWM duty cycle d_2. The input power refers to the ac power flowing out of the primary inverter, and the output power refers to the ac power flowing into the secondary inverter. In the preliminary experiment, d_1 is determined by the PI controller, and d_2 is varied in increments of 0.1 between 0 and 1. The phase difference between i_{1ac} and i_{2ac} is 90 deg. and the power flowing into the secondary inverter is minimum when $0.4 < d_2 < 0.5$. This indicates that the primary and secondary

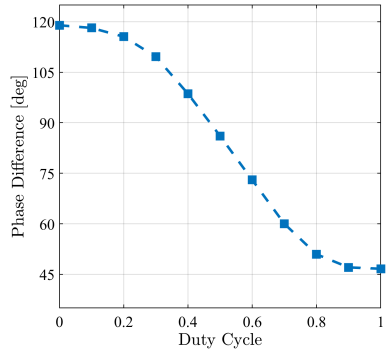

(a)

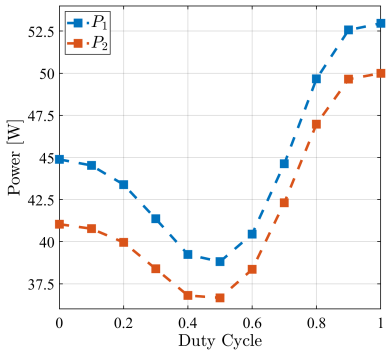

(b)

Fig. 5: (a) Phase difference between i_{1ac} and i_{2ac} measured as a function of d_2. (b) Input/output power measured as a function of d_2.

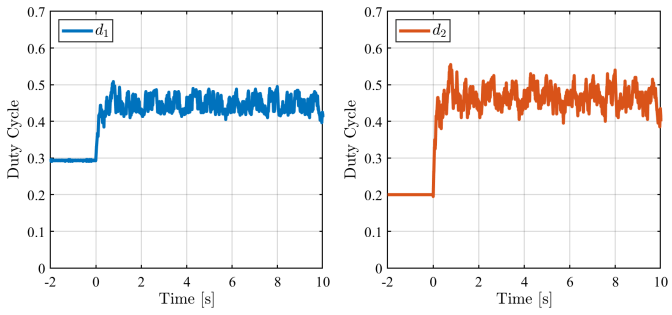

(a) (b)

Fig. 6: Experimental results of the trajectories of the PWM duty cycles d_1 and d_2 under the proposed control. (a) d_1. (b) d_2.

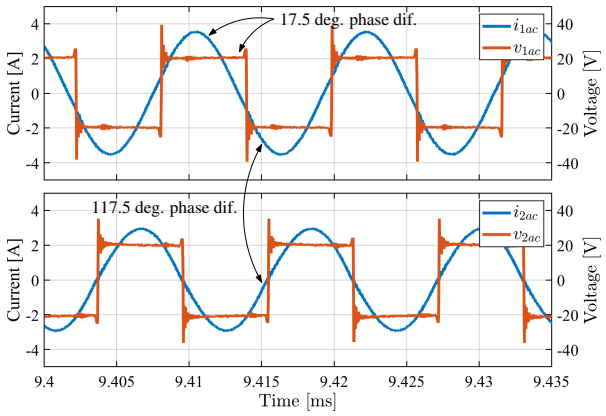

(a)

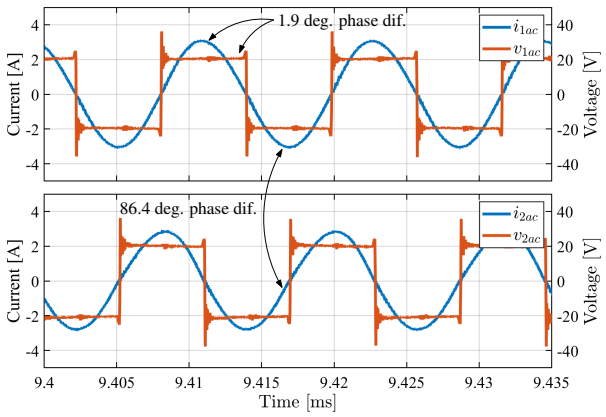

(b)

Fig. 7: Experimental waveforms of v_{1ac}, i_{1ac} and v_{2ac}, i_{2ac} with/without the proposed control. (a) w/o control. (b) w/ control.

TABLE II: COMPARISON OF PHASE DIFFERENCE.

	Phase dif. between v_{1ac} and i_{1ac}	Phase dif. between i_{1ac} and i_{2ac}
w/o control	17.5 deg.	117.5 deg.
w/ control	1.9 deg.	86.4 deg.

sides are perfectly tuned when $0.4 < d_2 < 0.5$. The results also indicate that the perfectly tuned state can be achieved by tracking the minimum power point in Fig. 5.

Fig. 6 shows the trajectories of d_1 and d_2 under the proposed control scheme of the switched capacitors. As shown in Fig. 3, d_1 is determined by the PI controller, and d_2 is determined by the MPT algorithm. The initial value of d_2 is set to 0.2, and the MPT algorithm starts at 0 s. By applying the MPT algorithm, d_2 settles between 0.4 and 0.5. This result shows consistency with the results in Fig. 5.

Fig. 7 shows the waveforms of v_{1ac}, i_{1ac} and v_{2ac}, i_{2ac} with/without the proposed control. The phase difference between v_{1ac} and i_{1ac} and the phase difference between i_{1ac} and i_{2ac} with/without the proposed control are listed in Table. II. The results without the control are obtained by disconnecting the MOSFETs from the switched capacitors so that C_{11} and C_{12} are connected in series on the primary side, and C_{21} and C_{22} are connected in series on the secondary side. By applying the proposed control, the phase difference between v_{1ac} and i_{1ac} becomes approximately 0 degrees, and the phase difference between i_{1ac} and i_{2ac} becomes approximately 90 degrees. This result verifies that the proposed control scheme can compensate X_1 and X_2 and autonomously tune the system.

V. Conclusion

In this paper, a control scheme of PWM-controlled switched capacitors is proposed to compensate for the self-inductance variations in WPT systems. The principle of the control scheme is explained based on the steady-state analysis of the WPT circuit. The system can be tuned autonomously by controlling the input phase angle on the primary side while tracking the minimum output power on the secondary side. The proposed control scheme does not require wireless communication or additional components besides the switched capacitors. The validity and performance of the control scheme are verified through experimental results.

The control scheme in this paper is derived based on a simplified circuit model of the WPT system. In fact, the circuit model assumes the primary and secondary dc link voltages to be symmetrical, and neglects the equivalent series resistance of the circuit. Therefore, further work needs to be done in terms of analysis and experimental verification in order to apply the control scheme to practical WPT systems.

Acknowledgement

This work was partly supported by JST-Mirai Program Grant Number JPMJMI21E2, JSPS KAKENHI Grant Number JP18H03768 and project JPNP21005, subsidized by the New Energy and Industrial Technology Development Organization (NEDO).

References

[1] R. Sedehi, D. Budgett, J. Jiang, X. Ziyi, X. Dai, A. P. Hu, and D. McCormick, "A wireless power method for deeply implanted biomedical devices via capacitively coupled conductive power transfer," *IEEE Transactions on Power Electronics*, vol. 36, no. 2, pp. 1870–1882, 2021.

[2] P. D. Hilario Re, S. K. Podilchak, S. A. Rotenberg, G. Goussetis, and J. Lee, "Circularly polarized retrodirective antenna array for wireless power transmission," *IEEE Transactions on Antennas and Propagation*, vol. 68, no. 4, pp. 2743–2752, 2020.

[3] V. Z. Barsari, D. J. Thrimawithana, and G. A. Covic, "An inductive coupler array for in-motion wireless charging of electric vehicles," *IEEE Transactions on Power Electronics*, vol. 36, no. 9, pp. 9854–9863, 2021.

[4] J. Kim, B. Clerckx, and P. D. Mitcheson, "Signal and system design for wireless power transfer: Prototype, experiment and validation," *IEEE Transactions on Wireless Communications*, vol. 19, no. 11, pp. 7453–7469, 2020.

[5] B. Ji, K. Hata, T. Imura, Y. Hori, S. Shimada, and O. Kawasaki, "Wireless power transfer system design with power management strategy control for lunar rover," *IEEJ Journal of Industry Applications*, vol. 9, no. 4, pp. 392–400, 2020.

[6] D. Kobayashi, K. Hata, T. Imura, H. Fujimoto, and Y. Hori, "Sensorless vehicle detection using voltage pulses in dynamic wireless power transfer system," in *EVS29 Symposium*, 2016, pp. 1–10.

[7] M. Sato, G. Yamamoto, D. Gunji, T. Imura, and H. Fujimoto, "Development of wireless in-wheel motor using magnetic resonance coupling," *IEEE Transactions on Power Electronics*, vol. 31, no. 7, pp. 5270–5278, 2016.

[8] H. Kim, J. Cho, S. Ahn, J. Kim, and J. Kim, "Suppression of leakage magnetic field from a wireless power transfer system using ferrimagnetic material and metallic shielding," in *2012 IEEE International Symposium on Electromagnetic Compatibility*, 2012, pp. 640–645.

[9] S. Y. Jeong, J. H. Park, G. P. Hong, and C. T. Rim, "Autotuning control system by variation of self-inductance for dynamic wireless ev charging with small air gap," *IEEE Transactions on Power Electronics*, vol. 34, no. 6, pp. 5165–5174, 2019.

[10] J. Lu, G. Zhu, and C. C. Mi, "Foreign object detection in wireless power transfer systems," *IEEE Transactions on Industry Applications*, vol. 58, no. 1, pp. 1340–1354, 2022.

[11] S. Y. Jeong, V. X. Thai, J. H. Park, and C. T. Rim, "Self-inductance-based metal object detection with mistuned resonant circuits and nullifying induced voltage for wireless ev chargers," *IEEE Transactions on Power Electronics*, vol. 34, no. 1, pp. 748–758, 2019.

[12] D.-H. Kim and D. Ahn, "Self-tuning lcc inverter using pwm-controlled switched capacitor for inductive wireless power transfer," *IEEE Transactions on Industrial Electronics*, vol. 66, no. 5, pp. 3983–3992, 2019.

[13] S. Ann and B. K. Lee, "Analysis of impedance tuning control and synchronous switching technique for a semibridgeless active rectifier in inductive power transfer systems for electric vehicles," *IEEE Transactions on Power Electronics*, vol. 36, no. 8, pp. 8786–8798, 2021.

[14] M. Ishihara, K. Fujiki, K. Umetani, and E. Hiraki, "Autonomous system concept of multiple-receiver inductive coupling wireless power transfer for output power stabilization against cross-interference among receivers and resonance frequency tolerance," *IEEE Transactions on Industry Applications*, vol. 57, no. 4, pp. 3898–3910, 2021.

[15] R. Mai, Y. Liu, Y. Li, P. Yue, G. Cao, and Z. He, "An active-rectifier-based maximum efficiency tracking method using an additional measurement coil for wireless power transfer," *IEEE Transactions on Power Electronics*, vol. 33, no. 1, pp. 716–728, 2018.

[16] A. Berger, M. Agostinelli, S. Vesti, J. A. Oliver, J. A. Cobos, and M. Huemer, "A wireless charging system applying phase-shift and amplitude control to maximize efficiency and extractable power," *IEEE Transactions on Power Electronics*, vol. 30, no. 11, pp. 6338–6348, 2015.

[17] R. Matsumoto, B. Ji, H. Fujimoto, and Y. Hori, "Resonance frequency adjustment using pwm-controlled variable capacitor for in-motion wpt with circuit parameter deviations," in *2020 IEEE PELS Workshop on Emerging Technologies: Wireless Power Transfer (WoW)*, 2020, pp. 158–163.